



LAWRENCE
LIVERMORE
NATIONAL
LABORATORY

Uranium passivation by C⁺ implantation: a photoemission and secondary ion mass spectrometry study

A. J. Nelson, T. E. Felter, K. J. Wu, C. Evans, J.
Ferreira, W. Siekhaus, W. McLean

March 29, 2005

Surface Science

Disclaimer

This document was prepared as an account of work sponsored by an agency of the United States Government. Neither the United States Government nor the University of California nor any of their employees, makes any warranty, express or implied, or assumes any legal liability or responsibility for the accuracy, completeness, or usefulness of any information, apparatus, product, or process disclosed, or represents that its use would not infringe privately owned rights. Reference herein to any specific commercial product, process, or service by trade name, trademark, manufacturer, or otherwise, does not necessarily constitute or imply its endorsement, recommendation, or favoring by the United States Government or the University of California. The views and opinions of authors expressed herein do not necessarily state or reflect those of the United States Government or the University of California, and shall not be used for advertising or product endorsement purposes.

Uranium passivation by C⁺ implantation: a photoemission and secondary ion mass spectrometry study

A. J. Nelson, T. E. Felter, K. J. Wu, C. Evans, J. L. Ferreira, W. J. Siekhaus and W. McLean
Lawrence Livermore National Laboratory, Livermore, CA 94550

Implantation of 33 keV C⁺ ions into polycrystalline U²³⁸ with a dose of 4.3×10^{17} cm⁻² produces a physically and chemically modified surface layer that prevents further air oxidation and corrosion. X-ray photoelectron spectroscopy and secondary ion mass spectrometry were used to investigate the surface chemistry and electronic structure of this C⁺ ion implanted polycrystalline uranium and a non-implanted region of the sample, both regions exposed to air for more than a year. In addition, scanning electron microscopy was used to examine and compare the surface morphology of the two regions. The U 4*f*, O 1*s* and C 1*s* core-level and valence band spectra clearly indicate carbide formation in the modified surface layer. The time-of-flight secondary ion mass spectrometry depth profiling results reveal an oxy-carbide surface layer over an approximately 200 nm thick UC layer with little or no residual oxidation at the carbide layer/U metal transitional interface.

Introduction

Preventing the corrosion and oxidation of uranium is important to the continued development of advanced nuclear fuel technologies. Knowledge of the surface reactions of uranium metal with various environmental and atmospheric agents, and the subsequent degradation processes, are vitally important in 21st century nuclear technology. A review of the oxidation of actinide elements and their use in catalysis [1] summarizes the present understanding of the kinetics and mechanisms of the reaction in dry and humid air.

Researchers have recently used N_2^+ and C^+ ion implantation to modify the near surface region chemistry and structure of uranium to affect the nucleation and growth kinetics of corrosion and to passivate the surface. [2-4] These researchers used Auger electron spectroscopy (AES) in conjunction with sputter depth profiling to show that the implanted surfaces had compositional gradients containing nitrides and carbides. Oxygen and molybdenum ion implantation has also been used to affect the hydriding properties and oxidation resistance of uranium. [5,6] In addition to chemical modification, ion implantation can create special reactive surface species that include defect structures that affect the initial adsorption and dissociation of molecules on the surface. Overall the modified surface layers provide mechanical stability and protection against further air corrosion.

This paper presents the results from an investigation of the surface chemistry, surface morphology and electronic structure of air-exposed C^+ implanted U. Examination of the resultant surface morphology with scanning electron microscopy (SEM) allowed a qualitative comparison between the implanted and the oxidized surfaces. Furthermore, core-level and valence band photoelectron spectroscopy in combination with time-of-

flight secondary ion mass spectrometry (ToF-SIMS) depth profiling provide a comprehensive characterization of the ion-implanted surface.

Experimental

Prior to implantation, the polycrystalline U was prepared with a final mechanical polishing step using 0.5 μm diamond paste that provided a near mirror finish. Initial oxidation of the U in laboratory air prior to introduction into the ion implanter vacuum chamber results in a ≤ 20 nm oxide. [7, 8] The specimen was firmly clamped to a water-cooled stainless steel block and sample heating during the implant was therefore minimal. The implantation was performed on the lightly oxidized U sample with a Varian 3000C ion implanter. The cryosorption pumps on the beamline and endstation maintained vacuum in the mid 10^{-6} to mid 10^{-7} Torr regime, respectively, during the implant. The implant was at normal incidence and CO_2 gas was used as the source material in the Freeman-type hot filament ionizer. The magnet separated the carbon +1 ions from the other ion species and the beam was rastered onto the surface in the standard fashion for ion implantation, and thus the dose is pure C, uniform and accurate to a few percent. The TRIM calculated sputtering rates of the surface oxygen and surface uranium by the implanting carbon ions are 44% and 23%, respectively. Note that the thin initial oxide layer (≈ 20 nm) was sputtered and modified during the ion irradiation. Part of the sample was masked to provide ready comparison of implanted versus non-implanted material. The contrast between implanted and non-implanted areas was readily and immediately seen visually, the implanted area being darker in appearance. With time, i.e. over a year in "standard" California environment (ambient temperature, 50% relative humidity), the

appearance of the implanted area remained unchanged. The non-implanted area, however, became progressively darker and lost its reflective properties. After approximately one year, the non-implanted area was darker in appearance than the implanted area.

X-ray photoelectron spectroscopy (XPS) was performed on a PHI Quantum 2000 system using a focused monochromatic Al $K\alpha$ x-ray (1486.7 eV) source for excitation and a spherical section analyzer. The instrument has a 16-element multichannel detection system. A 1 mm diameter x-ray beam was used for analysis. The x-ray beam is incident normal to the sample and the x-ray detector is at 45° away from the normal. The pass energy was 23.5 eV giving an energy resolution of 0.3 eV that when combined with the 0.85 eV full width at half maximum (FWHM) Al $K\alpha$ line width gives a resolvable XPS peak width of 1.2 eV FWHM. Deconvolution of non-resolved peaks was accomplished using Multipak 6.1A (PHI) curve fitting routines. The collected data were referenced to an energy scale with binding energies for Cu $2p_{3/2}$ at 932.72 ± 0.05 eV and Au $4f_{7/2}$ at 84.01 ± 0.05 eV. Binding energies were also referenced to the C 1s photoelectron line arising from adventitious carbon at 284.8 eV. XPS core-level analysis in combination with ion beam sputtering (1 kV Ar⁺, 3 x 3 mm) was performed to determine composition and bonding versus depth. The U sputter rate was estimated to be 2 nm/min. from SRIM-96 calculations. Low energy electrons and argon ions were used for specimen neutralization.

ToF-SIMS depth profile measurements were conducted in single-ion source mode. The liquid metal Ga ion gun was operated at 15kV and used for both sputtering and analysis. Raster areas for dc ion beam sputter and analysis are 200 μm x 200 μm and

50 μm x 50 μm , respectively. Since the sputter rate of the U substrate was not previously determined, the depth scale reported in these figures was converted using sputter rates for Si-based material. It is important to point out that significant ion mixing effects are expected under the 15kV Ga ion beam sputter. Such ion mixing can also reduce depth resolution as seen in the depth profile figures below.

Our experiments on the two regions of the sample show that the C^+ implantation greatly impedes the oxidation of the metal. For brevity, we describe region a of the sample and the corresponding figure panels (a) as non-implanted “oxidized” and region b of the sample and the corresponding figure panels (b) as “ C^+ Implanted.” The reader should keep in mind that regions a and b received the same exposure to ambient air, greater than one year.

Results

Low and high magnification planar view scanning electron microscopy (SEM) photomicrographs are presented in Figure 1(a) and (b), respectively, of the oxidized and air-exposed C^+ implanted U surfaces. The observed morphology on the surface of the oxidized Region A represents oxide island growth with subsequent lateral growth and coalescence (Stranski-Krastanov oxide growth). Closer examination of the non-implanted area shows a crack caused by the lattice mismatch strain at the interface between the oxide and metal.

The morphology of the C^+ implanted surface after one year in air appears less uniform (Region B) and exhibits no surface cracking. The enhanced surface roughness may be due to preferential oxide growth in certain regions. Surface chemistry, grain

boundary defects and inclusions exposed by polishing would affect oxide growth kinetics and may account for this observed morphology. Specifically, a surface inclusion larger than the thickness of the implanted layer would cause a discontinuity in the carbide layer thus allowing preferential oxidation to occur at that site.

Figure 2(a) shows the depth profile results from the non-implanted oxidized region. The total ion and oxygen ion profile remain steady after removal of surface contaminants and indicates the oxide is at least 100 nm thick (the limit of this experimental profile) on this non-implanted region after one-year exposure in ambient air. Also note that carbon and uranium carbide were both observed. Judging by the low signal intensities of the UC and UC₂ peaks and the slow growth of UC₂ peak intensity with depth, we attribute it to Ga⁺ sputter induced ion mixing. The observed UO signal mimics the O signal intensity with depth and is probably due to O diffusion into the bulk, especially along grain boundaries in this polycrystalline material. Fluorine was also observed and is probably due to either surface contamination from fluorocarbons or to the origin of the polycrystalline material. In this measurement of the oxidized surface, we did not sputter through the entire oxide thickness to reach the underlying metal.

Figure 2(b) presents the depth profile results from the 33keV, $4.3 \times 10^{17} \text{ cm}^{-2} \text{ C}^+$ implantation after air exposure. Notice the total ion level is no longer constant due to the elemental composition gradient in the implant layer. We observed a thin mixed oxy-carbide surface layer as indicated by the high oxygen and carbon content present in the first 50 nm of the surface. Arkush, *et al*, [2] and Musket [4] observed a similar trend in the near surface elemental composition of C⁺ implanted U with AES depth profiling. It is interesting to note that a fluorine rich region at 25nm was found. This is consistent with

the possible fluorine source discussed in Fig. 2(a). The carbon profile shows a well-defined implant layer between 25 – 225 nm with centroid at 125nm from the surface and a wide diffuse carbide/metal interface transition. This carbon profile is comparable to previous AES depth profile results [2, 4] and in good agreement with the implant depth determined by TRIM calculation.

Figures 3(a) and (b) presents the U $4f_{7/2,5/2}$ core-level spectra for the oxidized and air-exposed C⁺ implanted U surfaces, respectively, as a function of sputter etch time. The associated quantitative compositional analyses and elemental ratios versus depth are summarized in Table I as calculated using Multipak 6.1A (PHI) instrument specific relative sensitivity factors with measured core-level peak areas. The U $4f_{7/2,5/2}$ spin-orbit pair binding energies for the as received oxidized sample and 1 minute sputtered surfaces are 379.6 eV and 390.6 eV, respectively, and the full width at half maximum (FWHM) is between 1.8-2.2 eV. The binding energies are in agreement with literature values for uranium in a U⁴⁺ valence state. [9-13] The initial spectra for the as received oxidized surface also exhibits the shake-up satellite feature present 6.8 eV above the main U $4f_{7/2}$ peak that is typical for an oxidized surface. The phenomenon responsible for the shake-up satellites is the excitation of an electron from the O 2*p*-U bonding orbital to a partially occupied or unoccupied U 5*f* orbital. However, note that these satellite features are not present in the initial U $4f$ spectrum for the C⁺ implanted surface, but begin to appear after a 1 min. sputter etch.

Following further sputter depth profiling of both the air-exposed non-implanted and C⁺ implanted surfaces, the U $4f_{7/2}$ peaks broaden towards the lower binding energy side and the FWHM increases to 2.4 eV thus indicating the presence of multiple

oxidation states. Specifically, for the oxidized U surface, curve fitting results for the U $4f_{7/2}$ peak yields an additional component at 376.8 eV that represents the underlying metallic uranium. [10,13-15] In the case of the C⁺ implanted U surface, this broadening is much more pronounced and curve fitting yields two additional U $4f_{7/2}$ components at 376.8 eV and 378 eV. The binding energy of the additional component at 378 eV is in agreement with literature values for UC. [16-18] These features are mirrored in the U $4f_{5/2}$ region of the spectra and similar interpretations apply.

Note that the quantitative compositional analyses and elemental ratios summarized in Table I for the air-exposed C⁺ implanted U surface seem to indicate the presence of an oxy-carbide compound in support of Arkush, *et al*, proposed model. [2] These facts compliment the ToF SIMS results showing the presence of a thin oxy-carbide layer over the transitional U-carbide layer in the air exposed C⁺ implanted area, and a thicker oxide layer in the case of the non-implanted air exposed region.

The C 1s core-level spectra for the air exposed C⁺ implanted U surface versus sputter etch time is presented in Figure 4. Table I summarizes the quantitative compositional analyses and elemental ratios versus depth. The binding energy of the initial C 1s peaks for the implanted surface is 284.8 eV, representing C–H bonding, and 288.6 eV, representing O–C=O. Sputter depth profiling of the C⁺ implanted surface reveals a C 1s peak at 281.6 eV that is indicative of U-carbide, further supporting the interpretation of the U 4f results. [16,18] In addition, we note that the hydrocarbon peak intensity increased rapidly during XPS data acquisition thus showing the reactivity of the sputtered UC surface even in ultra-high vacuum.

Figure 5 shows the O 1s core-level spectra for both air-exposed regions. The initial O 1s doublet structure for both regions reveals the presence of adsorbed water. Specifically, the higher binding energy peak at 532.0 eV is indicative of adsorbed H₂O on the U-oxide surface. The lower binding energy peak at 529.8 eV represents the U-oxide. These results show that *ex-situ* adsorption of water on UO₂ does not cause dissociation in contrast to clean U metal. [11, 19] Also, comparing peak height ratios of the H₂O and oxide components in the initial O 1s spectra shows that more water vapor is adsorbed on the C⁺ implanted surface, which may be due to extra defect sites resulting from the implantation. Sputter etching of these two surfaces removes the adsorbed water and leads to an asymmetric O 1s peak shape. Further sputter etching of the C⁺ implanted surface leads to decreased O 1s peak intensity as the thin oxide overlayer is removed. These results are further summarized in Table I.

Figure 6 shows the valence band regions for the air exposed non-implanted and C⁺ implanted U surfaces. These spectra provide unique information about the electronic structure and the nature of chemical bonding in actinide materials. The lower valence band ($10 \text{ eV} < E_b < 50 \text{ eV}$) is defined by the U $6p_{3/2,1/2}$ - O $2s$ (C $2s$) electron region (lifetime broadening determines the U $6p$ line-shape) and the U $6s$ core-level. [20-24] For the oxidized surface, the U $6p_{3/2,1/2}$ binding energies are 17.2 eV and 27.8 eV, respectively, and the spin-orbit splitting of the U $6p_{3/2,1/2}$ doublet is 10.6 eV. These U $6p_{3/2,1/2}$ binding energies for the C⁺ implanted surface are shifted 0.2 eV to lower binding energy. Also note that the O $2s$ intensity is reduced and the U $6p_{3/2,1/2}$ branching ratio changes as we sputter etch into the U-carbide layer. Comparing the photoionization cross-sections for the C $2s$ and U $6p_{3/2}$ orbitals ($6.6 \times 10^{-4} \text{ Mb}$ and $8.2 \times 10^{-3} \text{ Mb}$,

respectively) [25] and noting that they overlap, the manifold peak intensity would be affected in the U-carbide layer thus explaining the changing branching ratio.

The upper valence band, $E_v < 10$ eV, consists of overlapping U $6d$ -L $2p$ states (L denotes ligand, e.g. O or C) and U $5f$ states located near the Fermi level. The O $2p$ and C $2p$ bands lie below the Fermi level and significantly hybridize with the U $5f$ and $6d$ bands. [18, 20-24] In addition to hybridization, the crystal field can split the d orbitals, thus leading to bonding and antibonding states. However, since the C $2p$ photoionization cross-section is negligible in comparison to those of the U $5f$ and $6d$ states [25] it is unlikely that we can observe these states with Al $K\alpha$ x-ray excitation. The observed broadening of the U $5f$ peak at the Fermi edge is more pronounced for the C^+ implanted surface. Since these data are acquired in the subsurface carbide layer, it suggests that the UC has metallic character. Further work using ultra-violet photoemission would have to be completed before a definitive conclusion could be drawn on the metallic character of UC.

Summary and Conclusions

Core-level and valence band photoelectron spectroscopy in combination with time-of-flight secondary ion mass spectrometry (ToF-SIMS) depth profiling have been used to characterize the air exposed U-carbide surface of C^+ implanted polycrystalline U. SEM analysis showed surface roughening without cracking and preferential oxidation following subsequent aging in air. Time-of-flight secondary ion mass spectrometry depth profiling results revealed a buried U-carbide layer and a wide diffuse carbide layer/U metal transitional interface. The wide defected transitional carbide layer strongly

suppresses oxidation as previously described. Core-level photoelectron spectroscopy clearly indicated carbide formation in the subsurface layer. Valence band electronic structure of the buried carbide layer indicates hybridization of the U *5f* and *6d* and ligand *2p* bands, and that it has metallic character. Future work will include probing the electronic structure of the buried carbide layer with soft x-ray fluorescence and x-ray absorption.

Acknowledgements

This work was performed under the auspices of the U.S. Department of Energy by the University of California Lawrence Livermore National Laboratory under Contract No. W-7405-Eng-48.

References

1. C.A. Colmenares, Prog. Solid State Chem. **15**, 257 (1984).
2. R. Arkush, M.H. Mintz and N. Shamir, J. Nucl. Mater. **281**, 182 (2000).
3. R. Arkush, M. Brill, S. Zalkind, M.H. Mintz and N. Shamir, J. Alloys Comp. **330-332**, 472 (2002).
4. R.G. Musket, Materials Research Society Conference Proceedings No. **93**, 49 (1987).
5. E.N. Kaufmann, R.G. Musket, C.A. Colmenares and B.R. Appleton, Materials Research Society Conference Proceedings No. **27**, 747 (1984).
6. R.G. Musket, G. Robinson-Weis and R.G. Patterson, Materials Research Society Conference Proceedings No. **27**, 753 (1984).
7. G.L. Powell, Y-12 Plant, Oak Ridge, Tennessee.
8. G.W. McGillivray, D.A. Geeson and R.C. Greenwood, J. Nucl. Mat. **208**, 81 (1994).
9. G.C. Allen, P.M. Tucker and J.W. Tyler, J. Phys. Chem. **86**, 224 (1982).
10. W. McLean, C.A. Colmenares, R.L. Smith, and G.A. Somorjai, Phys. Rev. **B25**, 8 (1982).
11. K. Winer, C.A. Colmenares, R.L. Smith, and F. Wooten, Surf. Sci. **177**, 484 (1986).
12. J.N. Fiedor, W.D. Bostick, R.J. Jarabek, and J. Farrell, Environ. Sci. Tech. **32(10)**, 1466 (1998).
13. S.V. Chong and H. Idriss, Surf. Sci. **504**, 145 (2002).
14. J.R. Naegele, J. Ghijsen and L. Manes, Struct. Bonding **59-0**, 197 (1985).
15. T. Gouder, C.A. Colmenares and J.R. Naegele, Surf. Sci. **342**, 299 (1995).
16. J. G. Dillard, H. Moers, H. Klewe-Nebenius, G. Kirch, G. Pfennig, and H. J. Ache, J. Phys. Chem. **88**, 5345 (1984).

17. T. Ejima, S. Sato, S. Suzuki, Y. Saito, S. Fujimori, N. Sato, M. Kasaya, T. Komatsubara, T. Kasuya, Y. Onuki, and T. Ishii, *Phys. Rev.* **B53**, 1806 (1996).
18. M. Eckle, R. Eloirdi, T. Gouder, M. Colarieti Tosti, F. Wastin, J. Rebizant, *J. Nucl. Mater.* **334**, 1 (2004).
19. M.N. Hedhili, B.V. Yakshinskiy and T.E. Madey, *Surf. Sci.* **445**, 512 (2000).
20. G.L. Goodman, *J. Alloys Compounds* **181**, 33 (1992).
21. T. Ejima, K. Murata, S. Suzuki, T. Takahashi, S. Sato, T. Kasuya, Y. Onuki, H. Yamagami, A. Hasegawa and T. Ishii, *Physica B* **186-188**, 77 (1993).
22. M. Kurihara, M. Hirata, R. Sekine, J. Onoe, H. Nakamatsu, T. Mukoyama, H. Adachi, *J. Alloys Comp.* **283**, 128 (1999).
23. G.H. Schadler, *Solid State Comm.* **74**, 1229 (1990).
24. T. Ito, H. Kumigashira, T. Takahashi, E. Yamamoto, Y. Haga and Y. Onuki, *J. Magn. Mater.* **226-230**, 40 (2001).
25. J.-J. Yeh and I. Lindau, "Atomic Subshell Photoionization Cross Sections and Asymmetry Parameters: $1 \leq Z \leq 103$ ", *Atomic Data and Nuclear Data Tables* **32**, 11 (1985).

Figure Captions

- Figure 1. SEM photomicrographs of polished uranium after exposure to air (a) low magnification showing non-implanted (oxidized) Region A and C⁺ implanted Region B. (b) 30,000X photomicrographs of the two regions.
- Figure 2. ToF-SIMS depth profiles (a) non-implanted (oxidized) and (b) air-exposed C⁺ implanted regions.
- Figure 3. XPS U 4f_{7/2,5/2} core-level spectra versus sputtered depth for the (a) oxidized and (b) air-exposed C⁺ implanted regions.
- Figure 4. XPS C 1s core-level spectra versus sputtered depth for the air-exposed C⁺ implanted region.
- Figure 5. XPS O 1s core-level spectra versus sputtered depth for the (a) oxidized and (b) air-exposed C⁺ implanted regions.
- Figure 6. Valence band spectra versus sputtered depth for the (a) oxidized and (b) air-exposed C⁺ implanted regions.

Table I. Relative XPS Compositional Analysis (atomic %) of the Oxidized and Air-exposed C⁺ Implanted Polycrystalline Uranium.

| Sample | U | O | C | O/U | C/U |
|---|----------|----------|----------|------------|------------|
| Oxidized, as received | 13.1 | 37.0 | 49.9 | 2.82 | 3.81 |
| Oxidized, 1 min. sputter | 29.4 | 36.1 | 34.5 | 1.23 | 1.17 |
| Oxidized, 3 min. sputter | 30.9 | 33.0 | 36.1 | 1.07 | 1.17 |
| Oxidized, 10 min. sputter | 32.2 | 30.1 | 37.7 | 0.93 | 1.17 |
| C ⁺ implanted, as received | 6.5 | 23.0 | 70.5 | 3.54 | 10.85 |
| C ⁺ implanted, 1 min. sputter | 32.5 | 44.7 | 22.8 | 1.38 | 0.70 |
| C ⁺ implanted, 3 min. sputter | 30.8 | 39.8 | 29.4 | 1.29 | 0.95 |
| C ⁺ implanted, 5 min. sputter | 30.1 | 35.5 | 34.4 | 1.18 | 1.14 |
| C ⁺ implanted, 10 min. sputter | 36.2 | 31.9 | 31.9 | 0.88 | 0.88 |
| C ⁺ implanted, 15 min. sputter | 35.8 | 27.8 | 36.4 | 0.78 | 1.02 |
| C ⁺ implanted, 24 min. sputter | 38.5 | 26.4 | 35.1 | 0.69 | 0.91 |

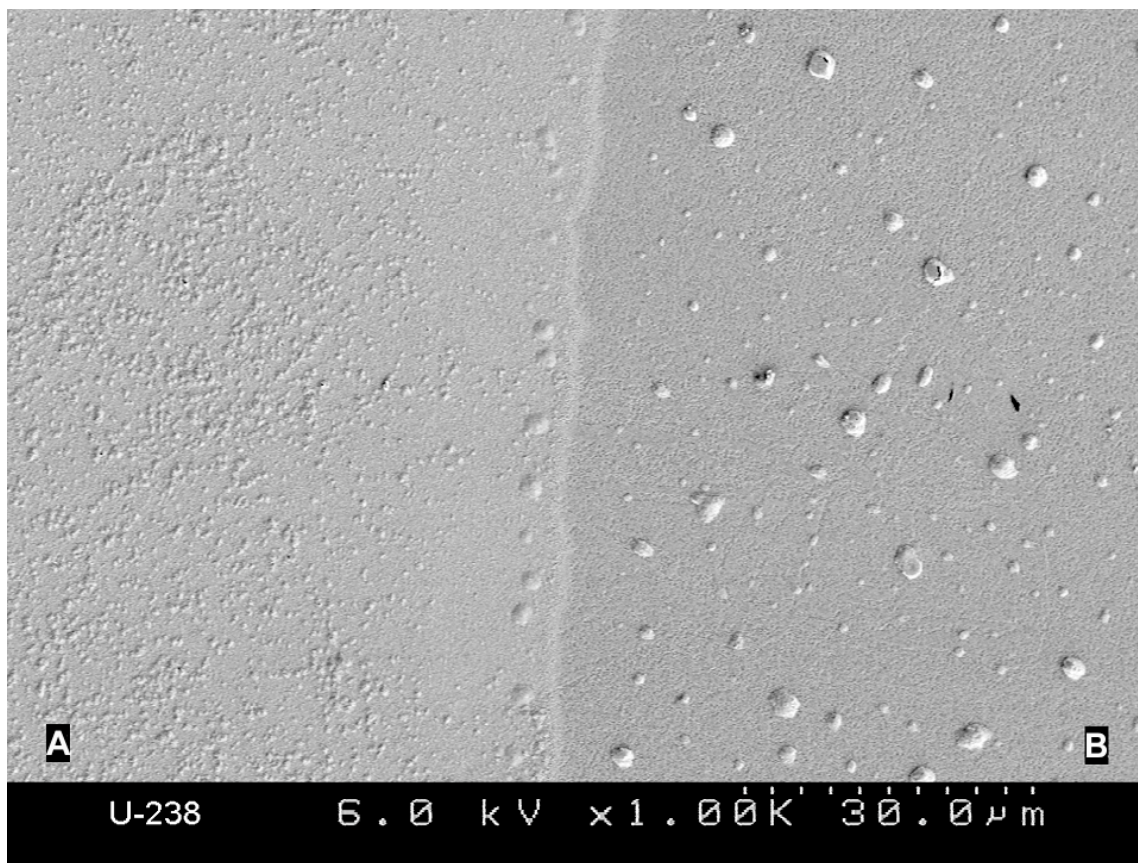


Figure 1(a).

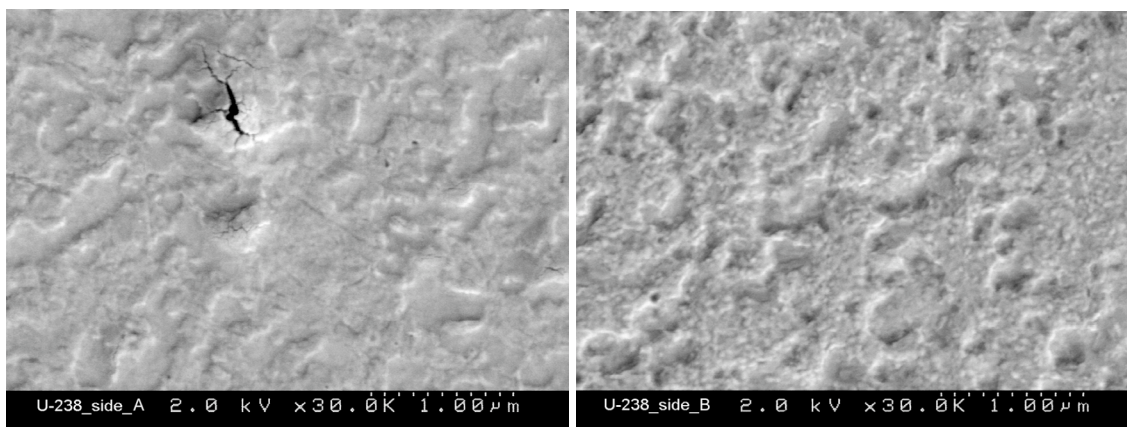


Figure 1(b).

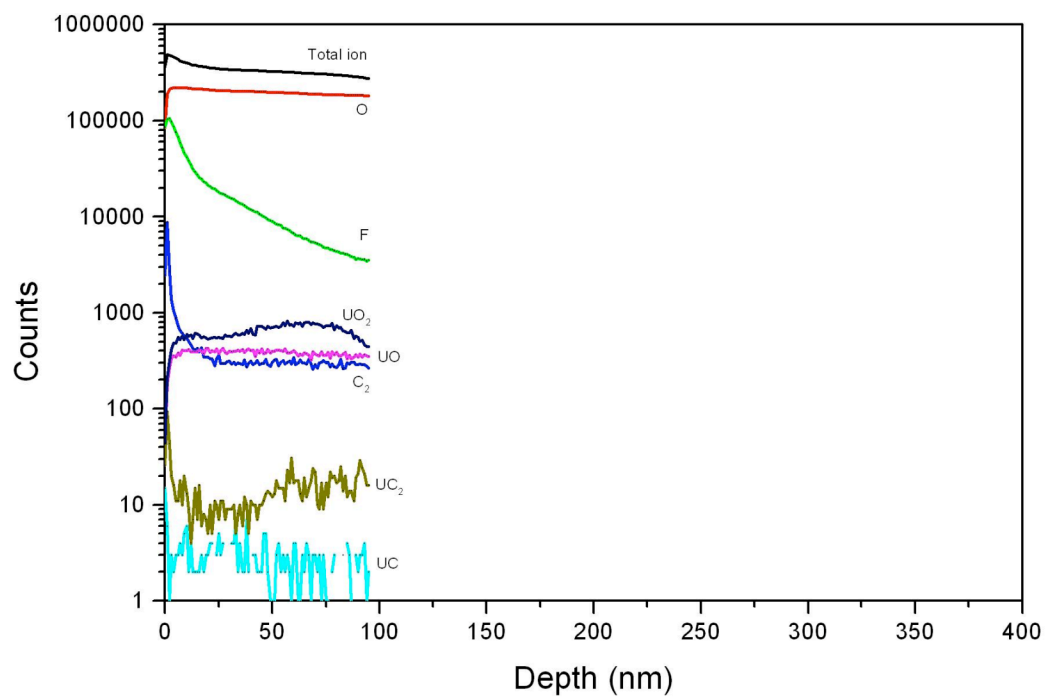


Figure 2(a).

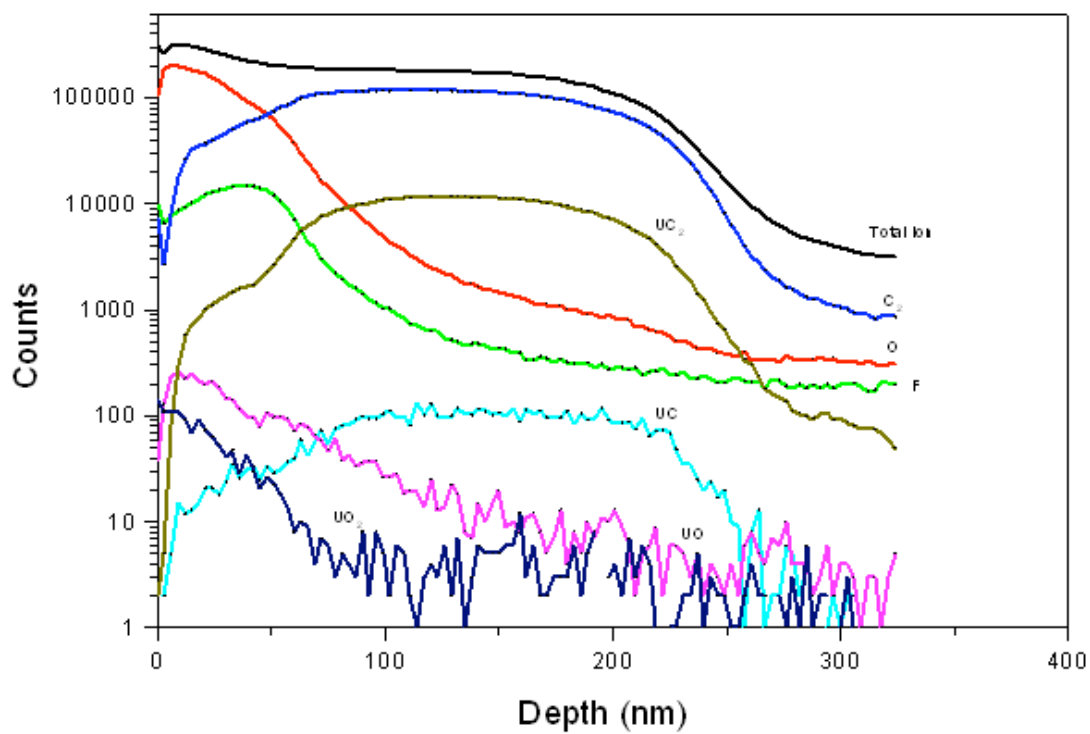


Figure 2(b).

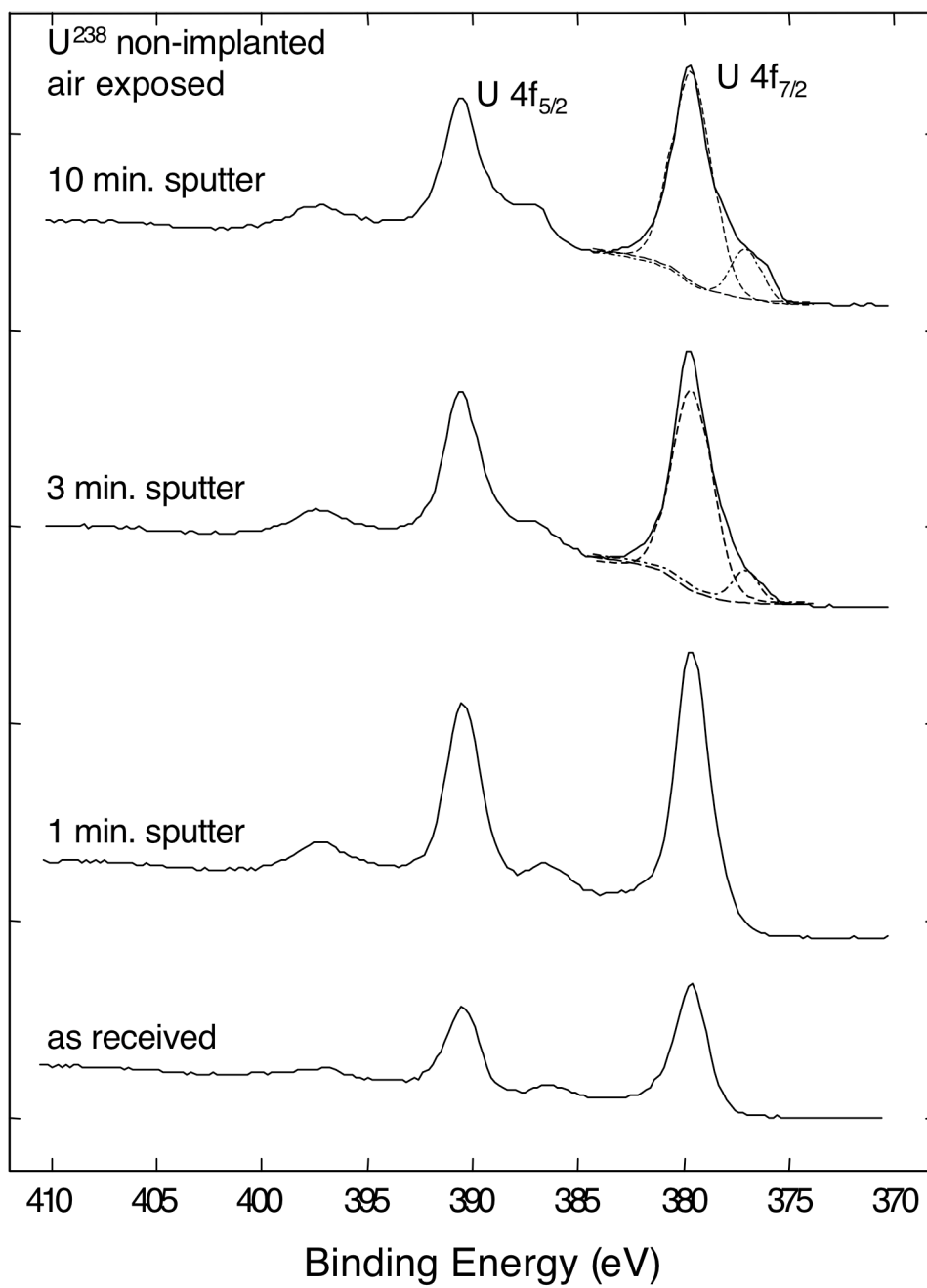


Figure 3(a).

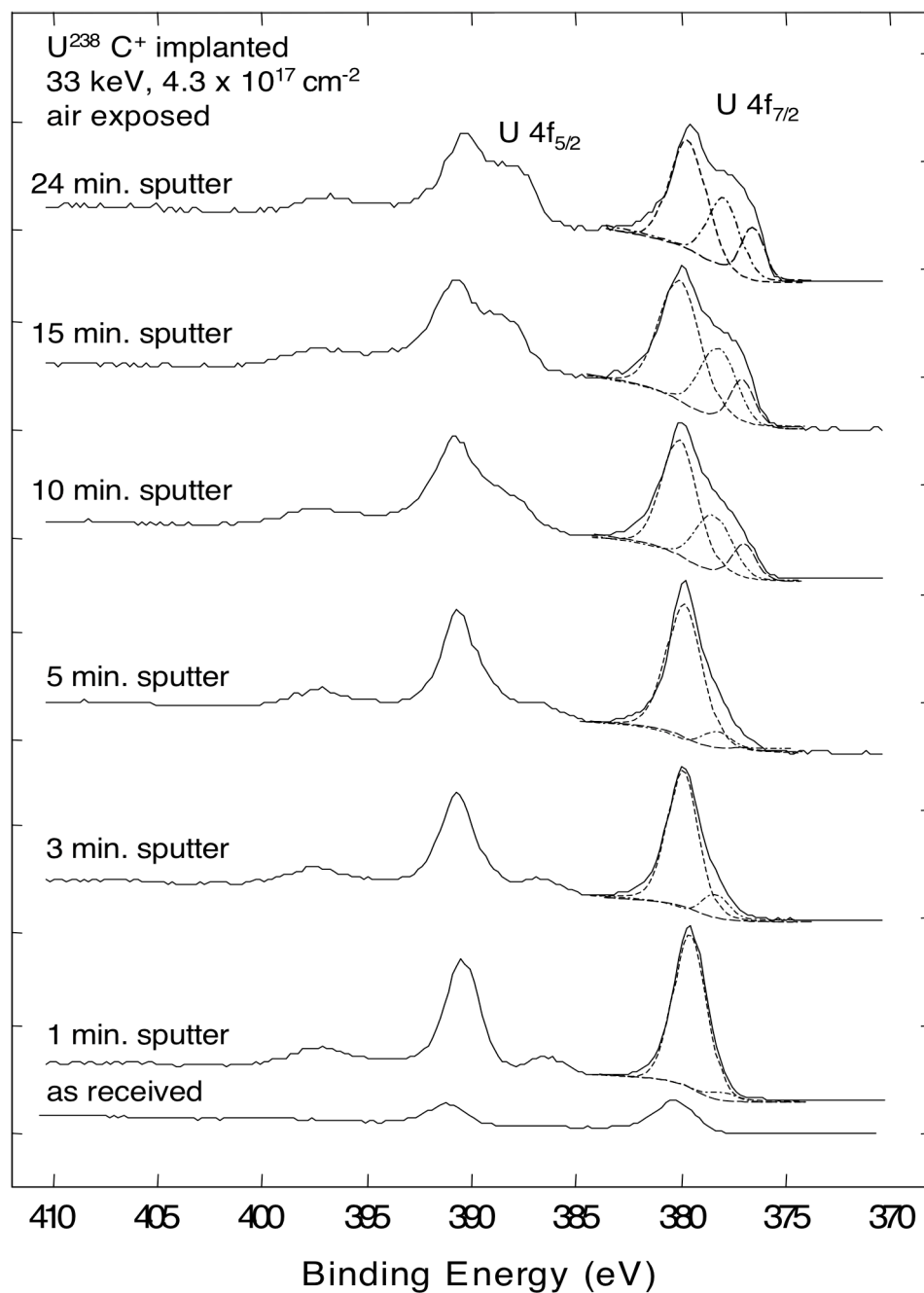


Figure 3(b).

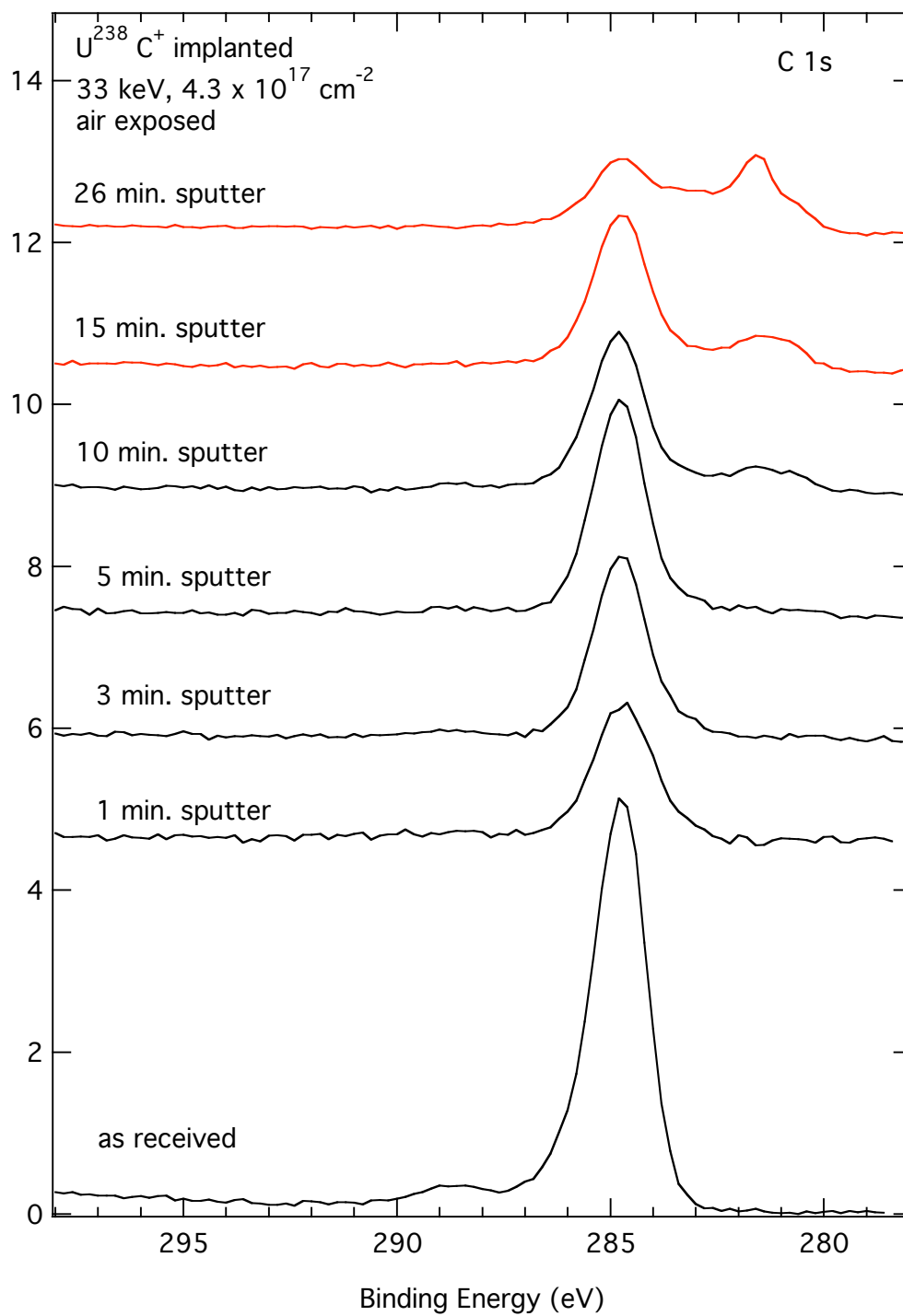


Figure 4.

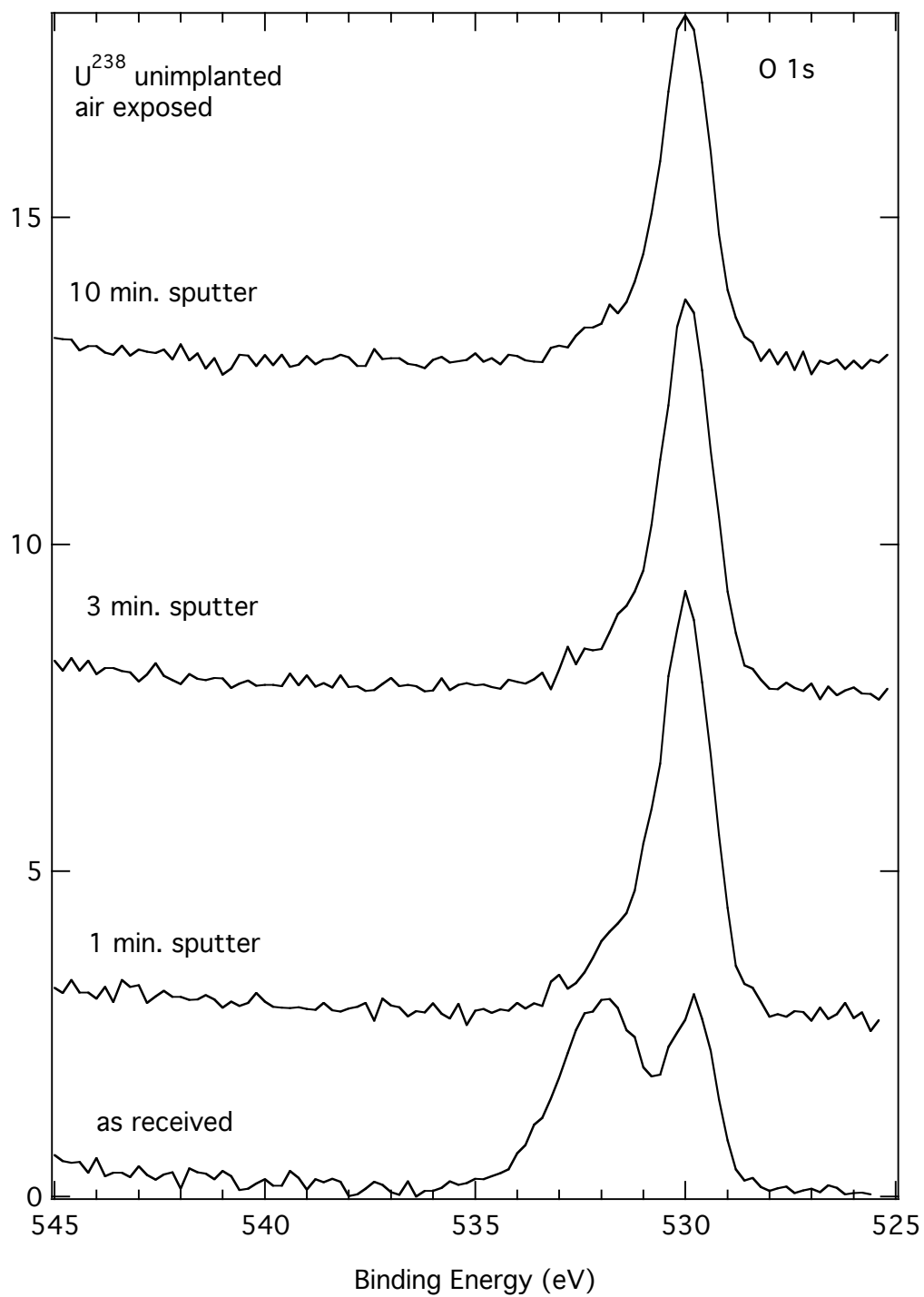


Figure 5(a).

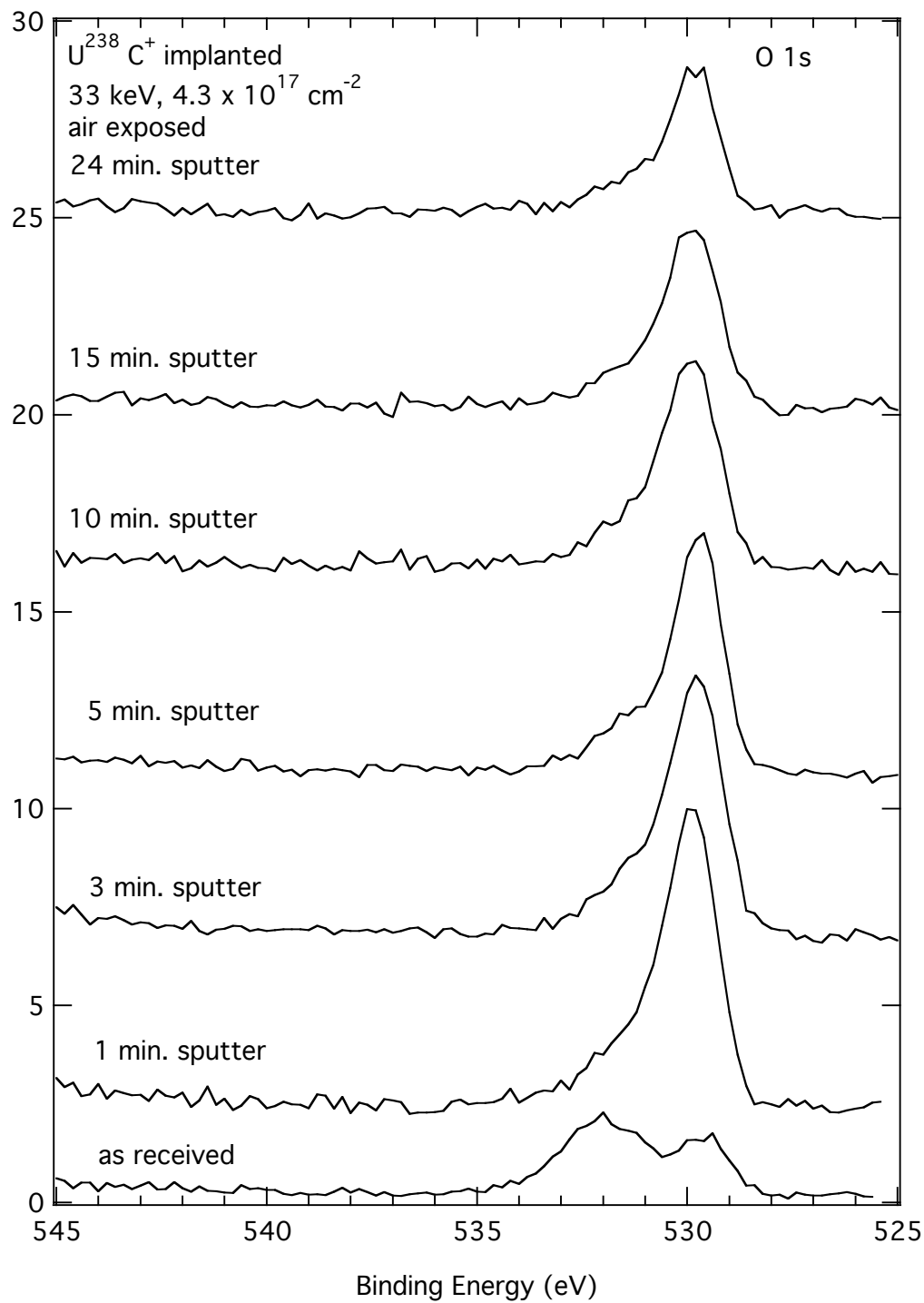


Figure 5(b).

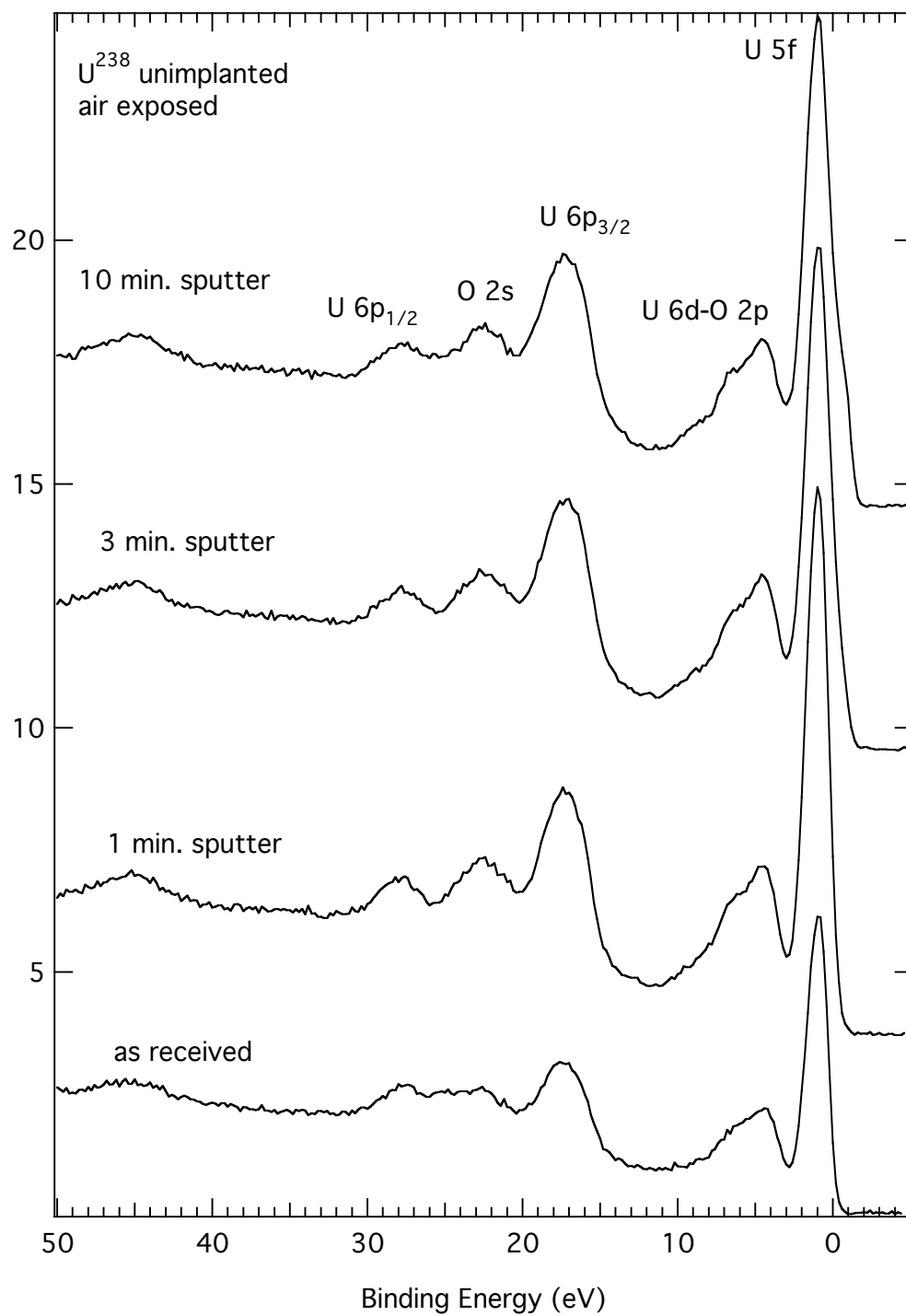


Figure 6(a).

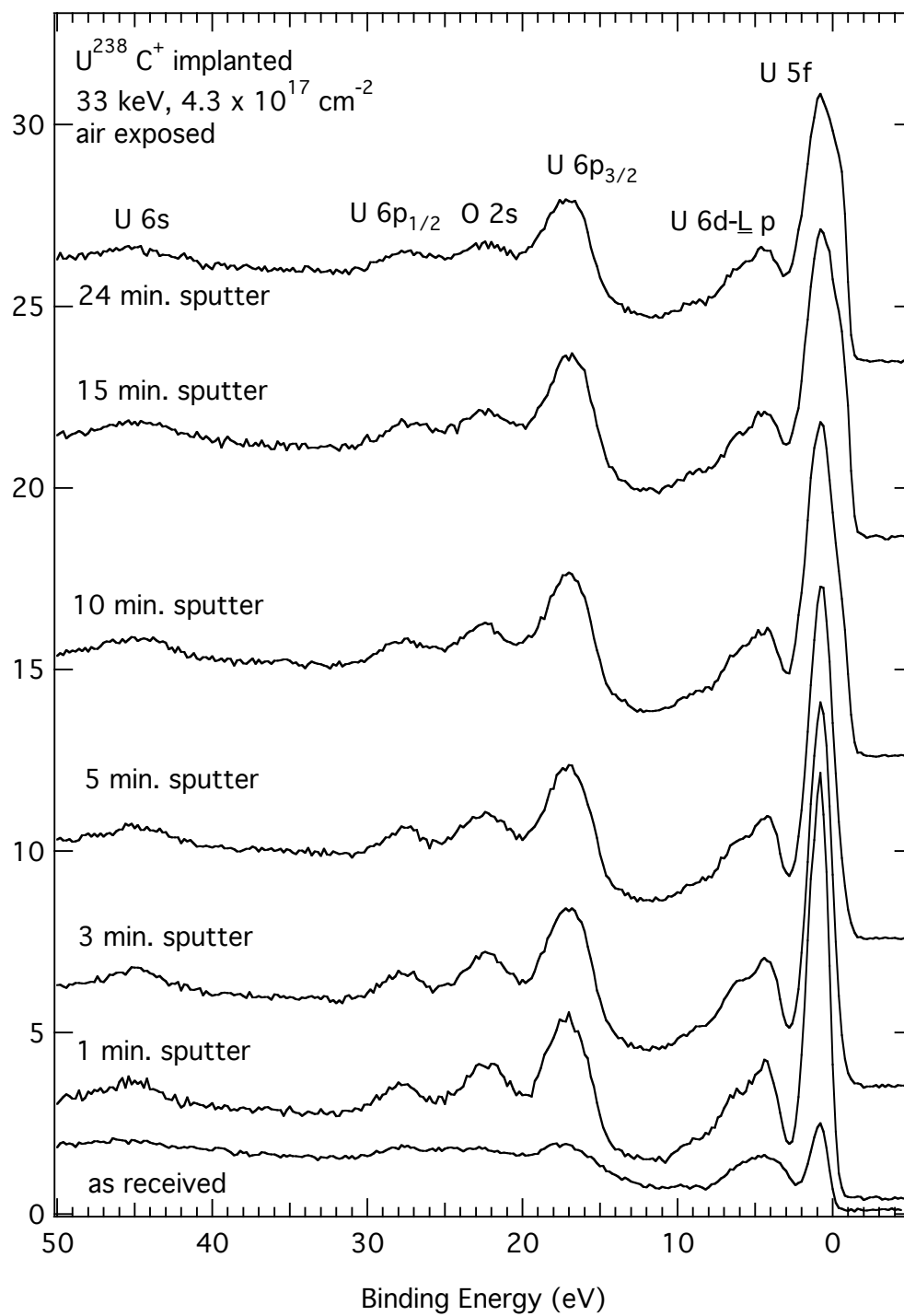


Figure 6(b).